International Journal of Modern Research in Engineering and Technology (IJMRET)
www.ijmret.org Volume 9 Issue 2 ǁ February 2024.

The Dynamic Modeling and Trajectory Tracking Control of an Unmanned Underwater Vehicle (UUV)

Gülten Yılmaz[1], Serhat Yılmaz[2]
[1](Electronic and Automation, Hereke Asım Kocabıyık High School/ Kocaeli University, Turkey)
[2](Electronic and Communication Engineering/ Kocaeli University, Turkey)

ABSTRACT : *This article presents the modeling and control of a four-degree-of-freedom (4-DOF), unmanned underwater vehicle (UUV) made of polyester, designed to be small and modular. Four fixed-position bidirectional thrusters—two for downward motion and two for horizontal planar motion—make up the propulsion system of the vehicle. Using the CAD program SolidWorks™, a thorough 3D model of the UUV was created in order to predict hydrodynamic parameters. Hydrodynamic coefficients were ascertained by boundary layer analysis using the computational fluid dynamics (CFD) program ANSYS Fluent. Under the right conditions, a 6-DOF dynamic model was created using the kinematic and hydrodynamic coefficients and reduced to a 4-DOF model. A PID control law divided into two parts was developed to keep the UUV in the desired path. PID controllers are widely used because they are both simple and easy to implement. However, for a dynamic and nonlinear system such as a UUV, controller gains need to be readjusted for each path. A fuzzy controller was designed to enable the UUV to track various trajectories without the need for manual gain adjustment for different trajectories. Both PID and fuzzy PID controllers for 3D trajectories were developed in Matlab/Simulink, and simulation studies were conducted. While the average value of position error during trajectory tracking for the PID controller is 0.057 m, the average value of position error for the fuzzy PID controller is 0.021 m.*

KEYWORDS – *PID Control, FLC, UUV, Dynamic Model*

I. INTRODUCTION

Unmanned Underwater Vehicles (UUVs) are robotic devices that can autonomously navigate underwater without human intervention, using built-in sensors, propulsion systems for navigation, and a built-in computer for decision-making [1]. A large part of the Earth's surface is covered with water bodies such as oceans, rivers, and lakes. These environments harbor a large portion of the world's natural resources, most of which remain undiscovered to this day. These natural resources have a direct and indirect impact on human beings. UUVs can be useful when conducting exploration to exploit natural resources such as seas and oceans for the benefit of humanity. Additionally, UUVs have potential uses in the marine sector as well as in the commercial, the army, and academic sectors [2]. Such unmanned underwater robotic systems are increasingly important for the exploration of vast and deep oceans and water bodies, as well as for environmental safety.

The UUV designed and subject to this study can be seen in Figure 1. The UUV consists of a cylindrical main body made of fiberglass composite material and two cylindrical battery compartments that are watertight. Four fixed bidirectional thrusters are used for the UUV's motion. Two of them are vertically centered on the sides of the vehicle, while the other two are located at the back of the vehicle. The vertical thrusters are used for lift, while the horizontal thrusters at the back are used for rolling and yawing. The robot has an Arduino Nano single-board microcontroller, sensors, a battery that recharges, a power management board, and a single camera configuration. This vehicle needs the proper system for navigation in order to operate as an unmanned underwater vehicle.

Unmanned Underwater Vehicles (UUVs) use algorithms and embedded sensor data to maneuver independently over difficult underwater settings. The accuracy of the navigation system depends on the

accuracy of the UUV's kinematic and dynamic model. Fossen presented a detailed kinematic and dynamic model for an underwater vehicle [3, 4]. Many researchers have presented different kinematic and dynamic models for various UUVs [5], [6], [7], [8].

Figure 1. 4-DOF underwater vehicle RedFin

In general, the correct hydrodynamic model of an underwater vehicle can determine and control the physical details of its operational dynamics [9]. It is evident that reducing parameter uncertainties in a precise underwater vehicle model can improve control performance. However, the cost of obtaining an accurate underwater vehicle model is often expensive using existing modeling methods. Predicting the correct model becomes even more challenging when the body structures of underwater vehicles are complex. Due to the high cost involved, only large organizations possess the capability to model underwater vehicles with high accuracy. The hydrodynamic model of an underwater vehicle typically has a nonlinear structure [10]. This implies that traditional control algorithms are often ineffective in addressing damping efforts under the assumption of low speed (ignoring cross-coupling damping terms and linear damping terms). Additionally, dynamic parameters are subject to uncertainties and are often different from the nominal model. For instance, the mass inertia matrix will increase when loads are added to the underwater vehicle. Unmodeled dynamics, environmental disturbances, and restoring effects also introduce uncertainties to the modeling process. Finally, sensor noise, signal transmission delays, and unmeasured states can affect control stability and tracking performance.

In trajectory tracking problems, an UUV is required to follow a pre-defined path by passing through specific points on the trajectory. These points are static and pre-defined, and the straight and curved lines connecting them form the path. Because of its simplicity and convenience of use, Line of Sight (LOS) guidance systems can be utilized to follow linear trajectories [11]. In studies addressing the control problems of different UUVs, from simple PD and PID [1, 12]. In nonlinear control applications, intelligent control approaches such as [13], adaptive control [14], fuzzy control [15] and neuro-fuzzy control can be encountered. Fangui and colleagues have proposed a Fuzzy Sliding Mode (FSM) controller for the trajectory control of an autonomous underwater vehicle (AUV) in the horizontal plane. This controller can address the chattering issue of traditional Sliding Mode (SM) controllers for UUV's and enhance the accuracy of trajectory tracking [16]. In their study conducted by Xie and Zhu (2023), they proposed a progressive model predictive controller (MPC) for the trajectory control of an Autonomous Underwater Vehicle (AUV) [17]. In the progressive MPC, they applied a quantum-behaved particle swarm optimization algorithm based on nonlinear diminishing contraction-expansion coefficients to optimize the controller's output. Through various validation and comparative simulations, it was observed that the controller exhibited advantages in terms of accuracy, convergence, and stability. Because they are the most widely used, PID controllers are straightforward and simple to use. [18]. However, they cannot adjust to disturbances or changes in the environment; instead, they must be set for certain operating conditions. According to Carrasco et al. [8], Hammad et al. [5] adaptive controllers like Fuzzy-PID are therefore recommended for severe underwater conditions.

Fuzzy controllers are rule-based controllers that leverage expertise from human knowledge. Without the knowledge of the physical model of the system, they use a rule-based reasoning base to predict the required control signal [19]. The main disadvantage of FLC is that it requires tuning for many parameters such as the ranges and shapes of membership functions. In contrast, PID has only three parameters. Additionally, due to complex operations, FLC requires more computation time compared to traditional PID. Despite FLC not having significantly better characteristics in the time domain than PID, its main advantage is its ability to work with nonlinear systems [20].

In this study, a combination of FLC and PID has been utilized. This method combines the simple mathematical equations and low computation time of the PID controller with the ability of FLC to adjust and

adapt the PID parameters, allowing the PID controller to work with nonlinear systems. By comparing it with traditional PID, the time-domain performance and the function of the self-tuned Fuzzy PID controller (FPID) are demonstrated. A combination of trapezoidal and triangular inputs for fuzzy membership function design, along with bell-shaped functions for outputs, has been used. The fuzzy rules in this study have been adapted from the work of Sahoo et al. [21], demonstrating successful tuning behavior. The purpose of using bell-shaped membership functions is to obtain a nonlinear response due to the nonlinearity of AUV system dynamics and hydrodynamics [22]. The variation ranges of input and output membership functions have been determined taking into account the maximum position and velocity errors obtained from experimental studies.

The focus of this study is to address both modeling and robust control issues simultaneously with the aim of creating an effective and accessible underwater vehicle control system. With this study, it is aimed to contribute to the literature by proposing an adaptive controller for the robust control of a nonlinear system operating under unknown and challenging disturbances.

The scope of the study is presented in six sections. Section 1 consists of an introduction and literature review. In Section 2, the kinematic and dynamic model of the UUVs , section 3 is developed along with the estimation of system parameters, section 4 is closed-loop control system designed for the UUVs trajectory tracking are explained. In Section 5, control simulations have been described and in Section 6, results and recommendations are presented.

II. KINEMATIC AND DYNAMIC ANALYSIS OF UUV'S

The kinematic and dynamic modeling of a small underwater vehicle is covered in this section. The vehicle's mobility is provided by four fixed-position bi-directional thrusters. Kinematic analysis looks at the motion of the vehicle without taking the forces causing it into account. The forces causing the vehicle to move are also examined in a dynamic analysis.

2.1.Kinematic Modeling

The kinematic model of an underwater vehicle is a mathematical correlation that relates the vehicle's position, orientation, linear and angular velocities, and acceleration to an inertial frame fixed to the vehicle body. If the solid body structure of the UUVs is considered as a single manipulator fixed to an inertial coordinate frame fixed to the ground, its kinematic model with respect to the inertial frame (E-frame) is shown in Fig. 2. The frame fixed to the vehicle body (B-frame) is attached to the vehicle's geometric center along the heave, sway, and surge directions. The North-East-Down directions align with the inertial frame fixed to the earth (E-frame) or the inertial (x, y, z) frame, which is fixed to a location on the water's surface.

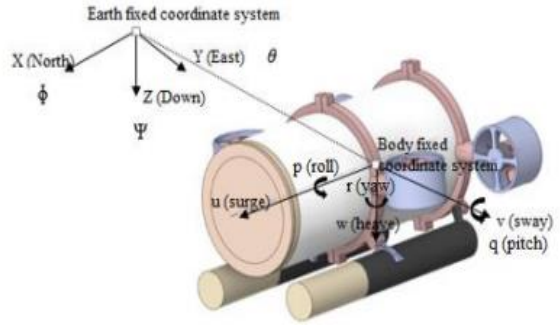

Figure 2. UUV earthcentric and bodyframe axes

Here; x, y, and z are the positions with respect to the fixed coordinate axis, and ϕ, θ, and Ψ are the rotational angles about these axes. The position and orientation vector of the UUV's with respect to the fixed coordinate axis is expressed as $\eta = [\eta_1, \eta_2]^T$, where $\eta_1 = [x, y, z]^T$ and $\eta_2 = [\phi, \theta, \Psi]^T$. The linear and angular velocity vectors, defined with respect to the coordinate axes located at the center of gravity of the UUV's, are given by $v_1 = [u, v, w]^T$ and $v_2 = [p, q, r]^T$, respectively.

Positions and orientations defined in the fixed frame of reference : $\eta = [x, y, z, \phi, \theta, \Psi]^T$, Linear and angular velocities defined in the body-fixed frame : $v = [u, v, w, p, q, r]^T$.

The vector correlation between the parameters in both frames can be defined using the Euler transform as Eq. (3).

$$J_1(\eta_2) = \begin{bmatrix} c\psi\, c\theta & -s\psi\, c\theta + c\psi\, s\theta\, s\varphi & s\psi\, s\varphi + c\psi\, s\theta\, c\varphi \\ s\psi\, c\theta & c\psi\, c\varphi + s\psi\, s\theta\, s\varphi & -c\psi\, s\varphi + s\psi\, s\theta\, c\varphi \\ -s\theta & c\theta\, s\varphi & c\theta\, c\varphi \end{bmatrix} \quad (1)$$

$$J_2(\eta_2)=\begin{bmatrix}1 & s\varphi\, t\theta & c\varphi\, t\theta\\ 0 & c\varphi & -s\theta\\ 0 & s\varphi/c\theta & c\varphi/c\theta\end{bmatrix} \quad (2)$$

$$\begin{bmatrix}\dot{x}\\ \dot{y}\\ \dot{z}\\ \dot{\varphi}\\ \dot{\theta}\\ \dot{\psi}\end{bmatrix}=\begin{bmatrix}J_1(\eta_2) & 0_{3x3}\\ 0_{3x3} & J_2(\eta_2)\end{bmatrix}\begin{bmatrix}u\\ v\\ w\\ p\\ q\\ r\end{bmatrix} \quad (3)$$

Here, c, s and t refer to cosine, sine and tangent functions, respectively. It should be noted that $J_2(\eta_2)$ is undefined at θ = ±π/2, It causes the kinematic equation to have a singularity. However, the pitch angle θ will never be close to ±π/2 for the current system. For a detailed kinematic and hydrodynamic model of an underwater vehicle, refer to Fossen (1995) [3].

2.2. Dynamic Modeling

A robot's position, velocity, and forces and moments are all related by a dynamic model. Accurate dynamic modeling is necessary for the control and navigation of an unmanned underwater vehicle (UUV). Fossen and Fjellstad have presented a nonlinear modeling approach for six degree-of-freedom vessels at sea, which can be expanded for an UUV model [22]. The correlation between different forces and torques involved in the motion of an UUV can be expressed as follows:

$$(M_{RB}+M_A)\dot{v}+(C_{RB}(v)+C_A(v))v+D_Lv+D_Q(v)v+g(\eta)=\tau \quad (4)$$

Here, M_{RB} is the fixed mass and inertia matrix of the UUVs, $M_A(v)$ is the added mass matrix due to the inertia of the surrounding fluid. $C_{RB}(v)$, is the rigid body's centripetal and coriolis matrix. $C_A(v)$ is the coriolis and centripetal matrix resulting from the rotation of the added mass. D_L and $D_Q(v)$ are linear and quadratic damping coefficient matrices respectively and containing the drag and lift terms, g(η) is the hydrostatic forces and moments matrix containing gravity and buoyancy forces, and τ is the vector of forces defined with respect to the body coming from the propulsion system.

Fixed mass - inertia matrix is:

$$M_{RB}=\begin{bmatrix}m & 0 & 0 & 0 & mz_G & -my_G\\ 0 & m & 0 & -mz_G & 0 & mx_G\\ 0 & 0 & m & my_G & -mx_G & 0\\ 0 & mz_G & my_G & I_{xx} & -I_{xy} & -I_{xz}\\ mz_G & 0 & -mx_G & -I_{yx} & I_{yy} & -I_{yz}\\ -my_G & mx_G & 0 & -I_{zy} & -I_{zy} & I_{zz}\end{bmatrix} \quad (5)$$

Here, m is the mass of the vehicle, (x_G, y_G, z_G) are the coordinates of the vehicle's center of gravity, and I's are the moments of inertia defined with respect to the coordinate frame fixed on the vehicle body.

Since the vehicle is balanced underwater, roll and pitch freedoms can be neglected. In this case, the M_{RB} matrix of the vehicle can be simplified as in Eq. (6).

$$M_{RB}=\begin{bmatrix}4.2 & 0 & 0 & 0 & 0 & 0\\ 0 & 4.2 & 0 & 0 & 0 & 0\\ 0 & 0 & 4.2 & 0 & 0 & 0\\ 0 & 0 & 0 & 0 & 0 & 0\\ 0 & 0 & 0 & 0 & 0 & 0\\ 0 & 0 & 0 & 0 & 0 & 0.087\end{bmatrix} \quad (6)$$

Similar to the simplification of M_{RB}, the added mass matrix M_A is also simplified to:

$$M_A = diag\{X_{\dot{u}}\ Y_{\dot{v}}\ Z_{\dot{w}}\ 0\ 0\ N_{\dot{r}}\} \quad (7)$$

Here $X_{\dot{u}}$, $Y_{\dot{v}}$, $Z_{\dot{w}}$ and $N_{\dot{r}}$ are the added mass coefficients and are related to the force and moment changes due to the acceleration of the vehicle in the relevant directions of movement.

The Coriolis and centripetal matrix of the rigid body is represented by the matrix $C_{RB}(v)$ of Coriolis and centripetal forces.

$$C_{RB}(v)=\begin{bmatrix}0 & 0 & 0 & c_{14} & c_{15} & c_{16}\\ 0 & 0 & 0 & c_{24} & c_{25} & c_{26}\\ 0 & 0 & 0 & c_{34} & c_{35} & c_{36}\\ c_{41} & c_{42} & c_{43} & 0 & c_{45} & c_{46}\\ c_{51} & c_{52} & c_{53} & c_{54} & 0 & c_{56}\\ c_{61} & c_{62} & c_{63} & c_{64} & c_{65} & 0\end{bmatrix} \quad (8)$$

Here,

$c_{14}=-c_{41}=m(y_Gq+z_Gr)$,
$c_{51}=-c_{15}=m(x_Gq-w)$,
$c_{61}=-c_{16}=m(x_Gr+v)$,
$c_{42}=-c_{24}=m(y_Gp+w)$,
$c_{25}=-c_{52}=m(z_Gr+x_Gp)$,
$c_{62}=-c_{26}=m(y_Gr-u)$,
$c_{43}=-c_{34}=m(z_Gp-v)$,
$c_{53}=-c_{35}=m(z_Gq+u)$,
$c_{36}=-c_{63}=m(x_Gp+y_Gq)$,

$c_{45} = -c_{54} = -I_{yz}q - I_{xz}p + I_z r$,
$c_{46} = -c_{64} = I_{yz}r + I_{xy}p - I_y q$,
$c_{56} = -c_{65} = -I_{xz}r - I_{xy}q + I_x p.$

Here, (x_G, y_G, z_G) are the coordinates of the center of gravity of the vehicle, m is the mass of the vehicle, and I is the moments of inertia in the directions indicated by the indices. In this study, the added coriolis matrix $C_A$is neglected since the vehicle moves at low speeds.

The hydrodynamic damping matrix $D(v)$ is the included the drag and lift terms and can be expressed as $D(v) = D_L + D_Q(v)$. Here, D_L is the linear damping matrix brought on by surface friction and potential damping and $D_Q(v)$ is the nonlinear damping matrix, v is the fluid velocity.

$$D_L = \begin{bmatrix} X_u & 0 & 0 & 0 & 0 & 0 \\ 0 & Y_v & 0 & Y_p & 0 & Y_r \\ 0 & 0 & Z_w & 0 & Z_q & 0 \\ 0 & K_v & 0 & K_p & 0 & K_r \\ 0 & 0 & M_w & 0 & M_q & 0 \\ 0 & N_v & 0 & N_p & 0 & N_r \end{bmatrix} \quad (9)$$

Quadratic axial drag is defined as:

$$X = -\left(\frac{1}{2}\rho C_d A_f\right) u|u| = X_{u|u|}u|u| \quad (10)$$

Here,$X_{u|u|} = \frac{dX}{d(u|u|)} = -\frac{1}{2}\rho C_d A_f$, where ρ is the fluid density in which the vehicle operates, C_d is the drag coefficient, and A_f is the surface area against the direction of motion.

$$D_Q(v) = diag(X_{u|u|}\, Y_{v|v|}\, Z_{w|w|}\, K_{p|p|}\, M_{q|q|}\, N_{r|r|}) \quad 11)$$

The matrix g(η) containing gravity and buoyancy forces is the vector of hydrostatic forces and moments that include the gravity and buoyancy forces.

$$g(\eta) = \begin{bmatrix} f_b + f_g \\ r_b x f_b + r_g x f_g \end{bmatrix} \quad (12)$$

Here, $f_g = [0, 0, W]^T$ where W = mg is the gravitational force defined with respect to the Earth-fixed frame. $f_b = [0, 0, -B]^T$. where B = ρg∇ is the buoyancy force defined with respect to the Earth-fixed frame. Additionally, g is the gravitational acceleration of 9.81 m/s^2, ρ is the water density, and ∇ is the volume of water displaced by the UUV.

$$g(\eta) = \begin{bmatrix} (W-B)\,s(\theta) \\ -(W-B)\,c(\theta)\,s(\phi) \\ -(W-B)\,c(\theta)\,c(\phi) \\ -(y_G W - y_b B)c(\theta)\,c(\phi) + (z_G W - z_b B)\,c(\theta)\,s(\phi) \\ (z_G W - z_b B)s(\theta) + (x_G W - x_b B)\,c(\theta)\,c(\phi) \\ -(x_G W - x_b B)c(\theta)\,s(\phi) - (y_G W - y_b B)\,s(\theta) \end{bmatrix} (13)$$

The vector of forces from thrusters fixed to the body is the force and torque matrix τ.

$$\tau = Lu \quad (14)$$

Here, L defines the thruster configuration.

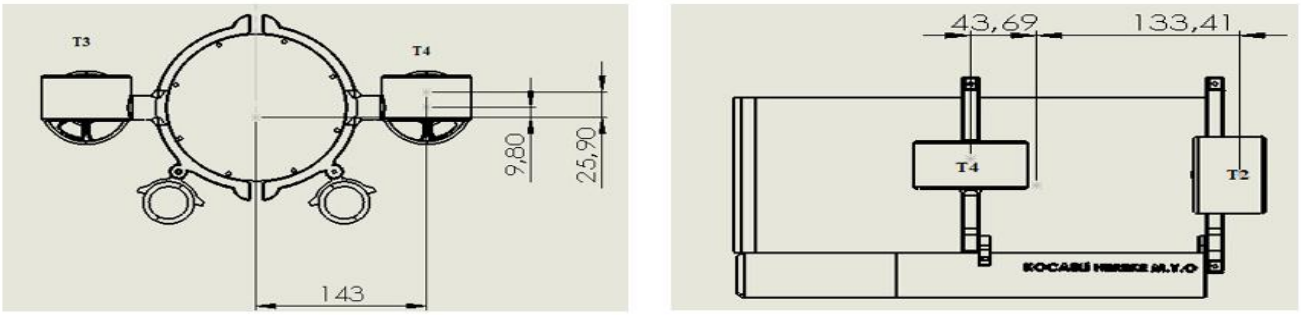

Figure 3. Positions of the motors on RedFin. Distances are given in millimeters

$$L = \begin{bmatrix} 1 & 1 & 0 & 0 \\ 0 & 0 & 0 & 0 \\ 0 & 0 & 1 & 1 \\ 0 & 0 & -L_{3y} & L_{4y} \\ L_{1z} & L_{2z} & L_{3x} & L_{4x} \\ -L_{1y} & L_{2y} & 0 & 0 \end{bmatrix} \quad (15)$$

"u" is the control input vector as well.

$$u = [T_1, T_2, T_3, T_4]^T \quad (16)$$

The UUV uses four bidirectional fixed thrusters for motion. In Figure 3, T1 and T2 represent two horizontal thrusters parallel to the horizontal plane used for horizontal translational motion, while T3 and T4 represent two vertical thrusters used for vertical translational motion, along with their positions. These position parameters are used to define the L matrix. Here, $L_{3y} = L_{4y}$ = 14,3 cm, $L_{1z} = L_{2z}$ = 0,98 cm, $L_{1y} = L_{2y}$= 14.3 cm and $L_{3x} = L_{4x}$ =4.37 cm.

III. SYSTEM PARAMETER ESTIMATION

The mechanical balance of the Roll and Pitch motions is achieved thanks to the relative position of the buoyancy and center of mass. However, since sway is not controlled and stabilized, free and uncontrolled motion (drift) is expected along the y-axis.

The following are some of the presumptions used in order to simplify the model, along with explanations for each:

- The UUV travels at a slow speed (maximum1.5 m/s)
- Because the UUV's structure is symmetric with respect to the x-z and x-y planes, during hydrodynamic operations, the x-z and x-y planes can be regarded as the symmetry planes.
- The lift forces have been disregarded because the UUV travels in the x-z and x-y planes at moderate speeds.
- The only environmental perturbation that can impact a fully submerged UUV is the underwater current. These disruption effects have been disregarded because the UUV will be evaluated in a swimming pool's static underwater environment. Hydrodynamic drag and propulsive forces are hence the forces operating on the UUV.
- Given that there is no water flow and that the heave and surge motions are independent, it is expected that the degree of freedom for vertical motion can be divided.
- Because the UUV stays horizontal throughout operations, there is no rolling or pitching action.

By making the aforementioned assumptions, the dynamic model can be simplified to a 4-DOF model with active control. This model includes surge, heave, sway, and yaw motions. Since degrees of freedom can be separated, a diagonal hydrodynamic damping matrix results. The external force matrix is regarded as nonexistent because the UUV floats neutrally. The following definition of the state vectors is based on the assumption that the roll and pitch are always zero:

Position and orientation in N-frame: $\eta = [x, y, z, \Psi]^T$, linear and angular velocity in B-frame: $v = [u, v, w, r]^T$ then kinematic model can be presented as:

$$\begin{aligned} \dot{x} &= u\cos(\Psi) - v\,sin(\Psi) \\ \dot{y} &= u\sin(\Psi) + v\,cos(\Psi) \\ \dot{z} &= w \\ \dot{\Psi} &= r \end{aligned} \quad (17)$$

And the dynamic model as Eq. (18):

$$\begin{bmatrix} m+X_{\dot{u}} & 0 & 0 & 0 \\ 0 & m+Y_{\dot{v}} & 0 & 0 \\ 0 & 0 & m+Z_{\dot{w}} & 0 \\ 0 & 0 & 0 & I_Z+N_{\dot{r}} \end{bmatrix} \begin{bmatrix} \dot{u} \\ \dot{v} \\ \dot{w} \\ \dot{r} \end{bmatrix} + \left\{ \begin{bmatrix} 0 & 0 & 0 & -m(x_g r+v) \\ 0 & 0 & 0 & -m(y_g r-u) \\ 0 & 0 & 0 & 0 \\ m(x_g r+v) & m(y_g r-u) & 0 & 0 \end{bmatrix} + \begin{bmatrix} X_u & 0 & 0 & 0 \\ 0 & Y_v & 0 & 0 \\ 0 & 0 & Z_w & 0 \\ 0 & 0 & 0 & N_r \end{bmatrix} + \begin{bmatrix} X_{u|u|}|u| & 0 & 0 & 0 \\ 0 & Y_{v|v|}|v| & 0 & 0 \\ 0 & 0 & Z_{w|w|}|w| & 0 \\ 0 & 0 & 0 & N_{r|r|}|r| \end{bmatrix} \right\} \begin{bmatrix} u \\ v \\ w \\ r \end{bmatrix} + \begin{bmatrix} 0 \\ 0 \\ 0 \\ -(x_G W - x_b B)c\theta s\varphi - (y_G W - y_b B)s\theta \end{bmatrix} = \begin{bmatrix} T_1+T_2 \\ 0 \\ T_3+T_4 \\ -l_{1y}T_1 + l_{2y}T_2 \end{bmatrix} \quad (18)$$

To complete the dynamic model, the parameters of mass, inertia, and damping need to be estimated. According to the assumptions, neglecting other degrees of freedom, it is sufficient to estimate the parameters corresponding to the heave, surge, sway and yaw degrees of freedom. The following parameters need to be estimated: the UUV's mass (m), weight (W), buoyancy (B), mass moments of inertia, thruster positions, and the locations of the center of gravity (C_G) and center of buoyancy (C_B) in the body frame (x_g, y_g, z_g). A CAD model of the vehicle makes it simple to determine these parameters. A detailed CAD model was developed using the SolidWorks™ software, utilizing the measured weights and dimensions of individual components. This CAD model was then used to find the necessary system parameters for kinematic and dynamic modeling. It was found that C_B and C_G are located at (-1.24, 0, 0) cm and (-1.24, -0.02, 0.309) cm, respectively, along the x, y, z axes from the origin. The positions of the horizontal thrusters relative to the origin are T1 (13.3, -14.3, 0.98) cm, T2 (13.3, 14.3, 0.98) cm, and the positions of the vertical thrusters relative to the origin are T3 (4.37, -14.3, 0.98) cm, T4 (4.37, 14.3, 0.98) cm. The estimated system parameters are listed in Table 1.

Table 1. Mass, volume, inertia and centers of gravity

Parameters	m	I_{xx}	I_{yy}	I_{zz}	x_G	y_G	z_G	∇	x_b
Values	4.2	0.06	0.046	0.087	0.0124	0.0210	0.309	0.002	0.0124
Units	kg	kgm^2	kgm^2	kgm^2	m	m	m	m^3	m

The drag coefficients were used to derive the hydrodynamic damping parameters. ANSYS Fluent simulations were utilized to acquire these parameters. The average drag forces that were derived from flow simulations at various velocities along the body's length (X-axis), such as 0.2, 0.5, 1, and 1.5 m/s, are shown in Table 2. Figure 4 shows the velocity contour obtained from the simulations.

Table 2. Drag forces and moments calculated with CFD flow analysis for 'surge', 'heave', and 'yaw' degrees of freedom at different velocity values

Velocity (m/s)	0.2	0.5	1	1.5
Surge (N)	0.6309	3.732	14.687	33.775
Heave (N)	1.081	6.445	26.801	59.864
Angular velocity (rad/s)	0.2	0.5	1	1.5
Yaw (N.m)	0.0016	0.0095	0.102	0.242

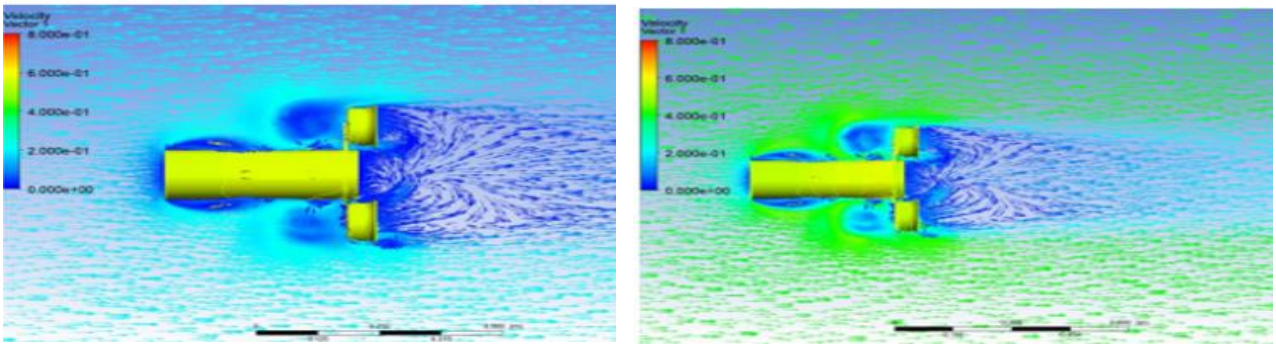

0.2 m/s 0.5 m/s

Figure 4. Velocity contour (for flow velocities of 0.2 m/s and 0.5 m/s (surge))

$$\text{Drag} = 15.354u^2 + 0.656u + 0.079 \quad (19)$$

Where 'u' in Eq. (19) stands for the velocity in the x-direction. Eq. (19), yields the following results for the linear (Xu) and quadratic (Xu|u|) damping terms along the X-axis: 0.656 and 15.354, respectively. Similar simulations were conducted for flow along the Z-axis (Fig. 5) and angular rotations around the Z-axis to determine the additional hydrodynamic damping factors.

Based on the thrust specifications, the thrust input parameters were chosen from the list supplied by the thruster manufacturer (Mitras Thruster : Degz Robotics) [23].

The parameters used in RedFin's dynamic model equation are seen in Table 3. The added mass values were estimated by the analytical calculation method by approximating the vehicle body to the cylinder. Damping coefficients were determined by the CFD method mentioned above.

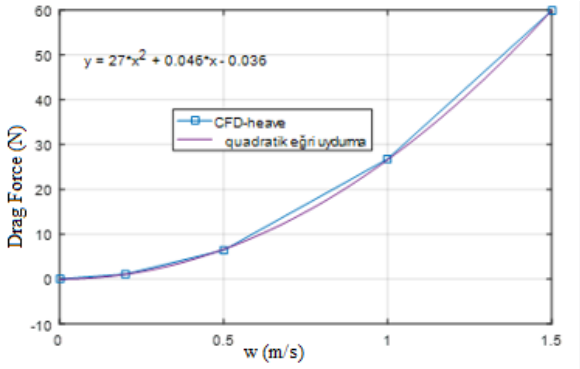

Figure 5. Variation of damping force calculated with CFD analysis for heave degree of freedom with respect to velocity

Table 3. Added mass, linear dampind and quadratic damping parameters for RedFin

Added Mass Coef.	$X_{\dot{u}}$	$Y_{\dot{v}}$	$Z_{\dot{w}}$	$K_{\dot{p}}$	$M_{\dot{q}}$	$N_{\dot{r}}$
	1.208	2.75	3.23	0.0149	0.0475	0.0359
Linear Damping Coef. (D_L)	X_u	Y_v	Z_w	K_p	M_q	N_r
	0.656	1.72	0.046	0.021	0.028	0.033
Quadratic Damping Coef. $(D_Q(v))$	$X_{u\|u\|}$	$Y_{v\|v\|}$	$Z_{w\|w\|}$	$K_{p\|p\|}$	$M_{q\|q\|}$	$N_{r\|r\|}$
	15.354	22.743	26.625	0.0487	0.1071	0.142

IV. CLOSED-LOOP CONTROL OF THE UUV'S

The thrust forces produced by the thrusters regulate the UUV's underwater propulsion, which must adhere to a specified trajectory To provide the needed thrust, a control system must therefore be able to anticipate the input signals that will be applied to the thrusters. The necessary thrust forces are calculated using a mathematical model of the system or from measurement data from position sensors. A closed-loop applications will assist in getting the UUV's trajectory tracking where it wants to go. The UUV is a nonlinear system consisting of interconnected 4-DOF (Degrees of Freedom). A partitioning control law is used to separate the

controller into two sections: the servo and model-based sections. The model-based component provides the system parameters (M_{RB}, C_{RB}, D_L, and D_Q), which are separate from the servo component.
The model's open-loop equation can be written like this.

$$(M_{RB} + M_A)\ddot{x} + C_{RB}\dot{x} + D_L\dot{x} + D_Q\dot{x} = f \quad (20)$$

The controller is divided into two parts. The model-based part utilizes M_{RB}, C_{RB}, D_L and D_Q. The model-based part decreases to a unit mass system, and the control gains of the servo section are adjusted based on unit mass.

The model-based component is as Eq. (21):

$$f = \alpha f' + \beta \quad (21)$$

The system's unit mass is represented by the following selection of α and β:

$$\alpha = M_{RB}, \quad \beta = C_{RB}\dot{x} + D_L\dot{x} + D_Q\dot{x} \quad (22)$$

In this case, the equation is $\ddot{x} = f'$.

The desired position and velocity can be obtained if the trajectory is specified as a twice differentiable function of time, xd(t). The formula for the positional error between the desired and actual positions is e=xd−x. The following is the PID control law that is used to determine f':

$$f' = \ddot{x}_d + K_d\dot{e} + K_p e + K_i \int e dt \quad (23)$$

Here, K_p, K_d, and K_i represent proportional, derivative, and integral control gains, respectively. If we combine this control law with Eq. (23):

$$\ddot{x} = \ddot{x}_d + K_d\dot{e} + K_p e + K_i \int e dt \quad (24)$$

$$\ddot{e} + \ddot{x}_d + K_d\dot{e} + K_p e + K_i \int e dt = 0 \quad (25)$$

The altered control law can be shown as follows when there is a continuous steady-state error:

$$\ddot{e} + \ddot{x}_d + K_d\dot{e} + K_p e + K_i \int e dt = f_{dist.} \quad (26)$$

Here, fdist represents a constant disturbance. The MATLAB/Simulink model of the path following controller with PID can be seen in Figure 6.

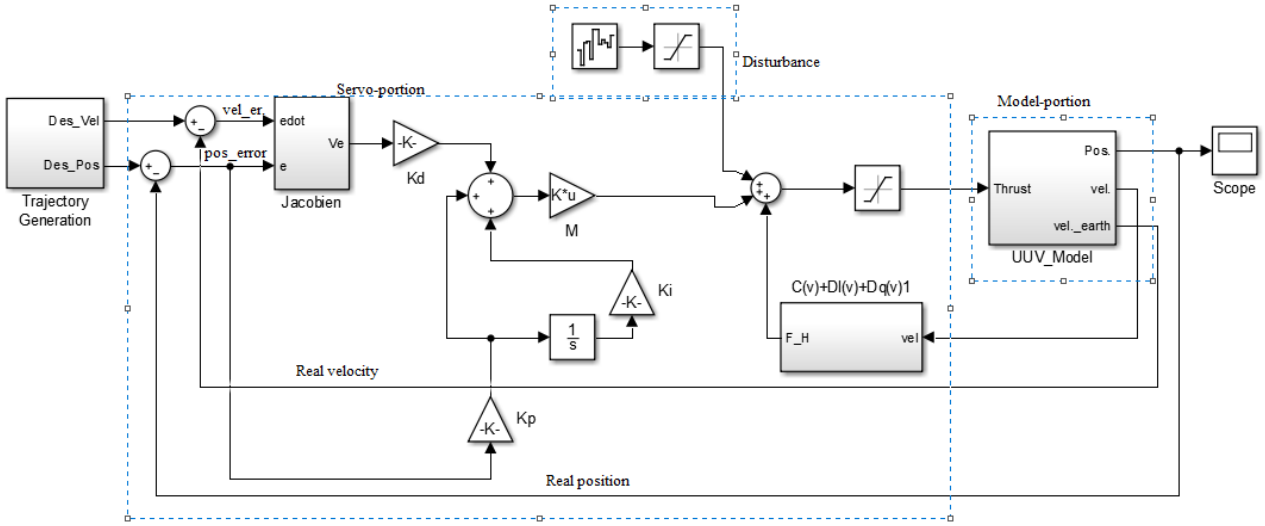

Figure 6. Path tracking PID control model for UUV

4.1. Self Tuning PID Controller By Fuzzy Logic

Due to the need for re-tunning PID controller gains for different trajectories, an adaptive structure is required to accommodate various paths and scenarios. There are several methods available in the literature to optimize the gains of traditional PID controllers,

including Artificial Neural Networks (NN), Genetic Algorithms (GA), Fuzzy Logic (FL), and Particle Swarm Optimization (PSO) [5], [12], [13], [14]. In this study, Fuzzy Logic Control (FLC) will be used for optimizing the PID gains. The use of FLC introduces adaptability to the controller and enhances its robustness. The Self-Tuning Fuzzy PID (STFPID) controller can be formulated as follows:

$$f'(t) = \left[K_p(t)e(t)\right] + \int_0^t [K_i(\tau)e(\tau)]d(\tau) + \frac{d[K_d(t)e(t)]}{dt} = [k_p^0 + \Delta k_p(t)]e(t) + \int_0^t \left[k_i^0 + \Delta k_i(\tau)\right]e(\tau)d(\tau) + \frac{d\left[k_d^0 + \Delta k_d(t)\right]e(t)}{dt} \quad (27)$$

Here, $K_p(t) = k_p^0 + \Delta k_p(t)$; $K_i(t) = k_i^0 + \Delta k_i(t)$; $K_d(t) = k_d^0 + \Delta k_d(t)$;; are the control gains with allowable variations.

k_p^0 , k_i^0, k_d^0 : Time-invariant constant gain values associated with the PID controller. $\Delta k_p(t)$ $\Delta k_i(t), \Delta k_d(t)$: Time-varying controller gains that change over the simulation period.

In this case, a Fuzzy Logic Controller (FLC) has been proposed to generate Δkp(t), Δki(t), and Δkd(t). FLC utilizes fuzzy linguistic variables, which represent Negative Large (NL), Negative Medium (NM), Negative Small (NS), Zero (ZR), Positive Small (PS), Positive Medium (PM), and Positive Large (PL), respectively. FLC has two inputs: the system error e(t) and the derivative of the error with respect to time. To generate the controller gains, FLC requires three outputs. Consequently, FLC has two inputs and three outputs, as shown in Figure 7.

In cases where the error is large, a large value of K_p is necessary to achieve a fast response. A smaller value of K_d can help avoid large instantaneous errors. A small Ki value will assist in preventing overshooting.

Table 4. FLC Rule Base for ΔKp(t) (Sahoo, 2020)

e / ė	NL	NM	NS	Z	PS	PM	PL
NL	PL	PL	PM	PM	PS	PS	Z
NM	PL	PL	PM	PM	PS	Z	Z
NS	PM	PM	PM	PS	Z	NS	NM
Z	PM	PS	PS	Z	NS	NM	NM
PS	PS	PS	Z	NS	NS	NM	NM
PM	Z	Z	NS	NM	NM	NM	NL
PL	Z	NS	NS	NM	NM	NL	NL

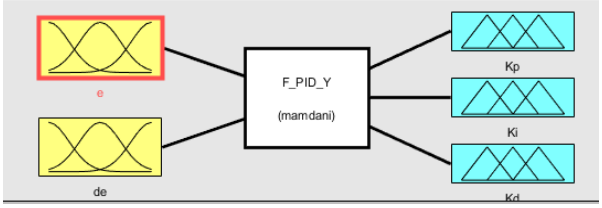

Figure 7. Fuzzy logic controller

Table 5. FLC Rule Base for ΔKi(t) (Sahoo, 2020)

e / ė	NL	NM	NS	Z	PS	PM
NL	PS	PS	Z	Z	Z	PL
NM	NS	NS	NS	NS	Z	NS
NS	NL	NL	NM	NS	Z	PS
Z	Z	Z	Z	Z	Z	Z
PS	NL	NM	NS	NS	Z	PS
PM	NM	NS	NS	NS	Z	PS
PL	PS	Z	Z	Z	Z	PL

Table 6. FLC Rule Base for ΔKd(t) (Sahoo, 2020)

e / ė	NL	NM	NS	Z	PS	PM
NL	NL	NL	NL	NM	NM	Z
NM	NL	NL	NM	NM	NS	Z
NS	NM	NM	NS	NS	Z	PS
Z	NM	NS	NS	Z	PS	PS
PS	NS	NS	Z	PS	PS	PM
PM	Z	Z	PS	PM	PM	PL
PL	Z	Z	PS	PM	PL	PL

When the error is of medium magnitude, the proportional gain (Kp) should be decreased in order to provide a quick system response and to have a small overshoot. A high value of the derivative gain (Kd) increases the speed of the system response, while the integral gain (Ki) should be appropriate to reduce steady-state error. When the error is of small magnitude, Kp and Ki should be large in order to ensure the system has ideal static performance. Taking these facts into account, fuzzy rules for Kp, Ki, and Kd are designed as presented in Tables 4, 5, and 6.

The membership functions used for inputs and outputs are respectively triangular (trimf) and bell curve (gbellmf) as shown in Figure 8. The FLC input and output ranges and parameter values for the membership functions are presented in Table 7. The STFPID controller designed in Matlab/Simulink is shown in Figure 9.

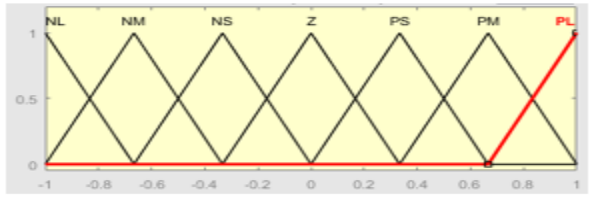

(a)

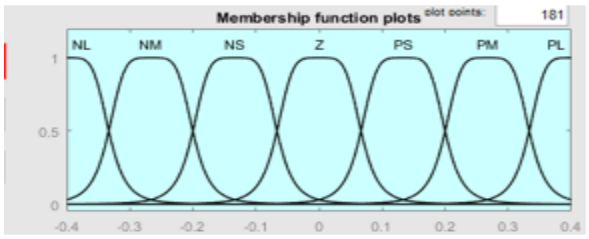

(b)

Figure 8. Membership Functions for Input and Output Variables (a) trimf and (b) gbellmf

The ranges of input/output parameters of the Fuzzy Logic Controller are shown in Table 7. These values were determined by taking into consideration previous studies and experimental measurements.

Table 7. FLC Input/Output Parameter Ranges

	$\dot{e}$	e	$\Delta k_p(t)$	$\Delta k_i(t)$	$\Delta k_d(t)$	k_p^0	k_i^0	k_d^0
x	[-1 1]	[-0.5 0.5]	[-5 5]	-	[-8 8]	12	-	16.8
y	[-0.8 0.8]	[-1 1]	-0.4 0.4]	[-0.04 0.04]	[-2 2]	0.707	0.1	1.72
z	[-0.3 0.3]	[-0.6 0.6]	[-10 10]	-	[-15 15]	16	-	30.52
Ψ	[-4 4]	[-1100 1100]	[-95 95]	-	[-50 50]	198	-	92

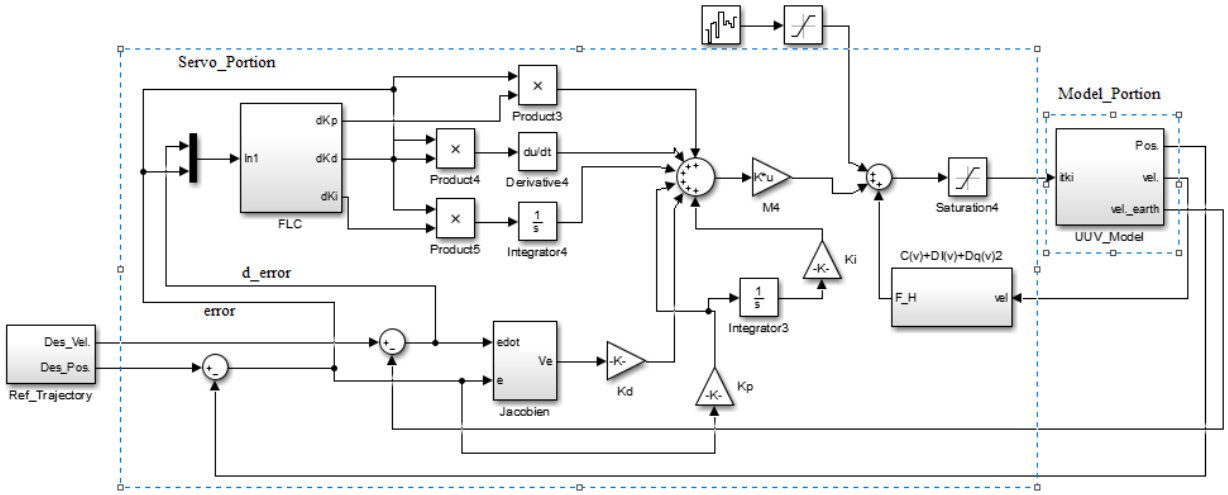

Figure 9. STFPID Controllör Simulink Model

V. CONTROL SIMULATIONS

First of all, the designed PID controller was simulated. Simulations were made for a circular 2D road. It was then simulated by drawing a circle with a diameter of 4 m and following a spiral trajectory in which it descended to a depth of 15 m from the water surface. The location tracking results are presented in Figure 10 and Figure 11, respectively. The equations for the circular path are x = 2sin(0.25t) and y = 2cos(0.25t). The equations for the 3D orbit are: x = 2sin(0.25t), y = 2cos(0.25t) and z = -0.5t. The adjusted control gains for the PID controller for this 3D path are presented in Table 8.

The gain values of the PID and STFPID controllers (both untuned and tuned) used for controlling the position and velocity values of the four degrees of freedom are shown in Table 9.

Table 8. Designed PID controller gain parameters

position	Kp	Ki	velocity	Kd
x	10	0	u	17.8
y	0.71	0.1	v	1.7
z	15	0	w	30.5
Ψ	200	0	r	90

The developed STFPID controller was simulated in MATLAB Simulink for tracking 2D and 3D trajectories.

It was observed that the controller successfully tracked the different trajectories more effectively compared to the conventional PID controller. The table 9 shows the controller gain parameters for both controllers that were used in this simulation. The gain values of the PID controller, which were tuned to track the 2D trajectory, did not exhibit sufficient tracking performance for the 3D trajectory since they were not retuned. However, the Self Tuning Fuzzy PID controller successfully tracked this different trajectory.

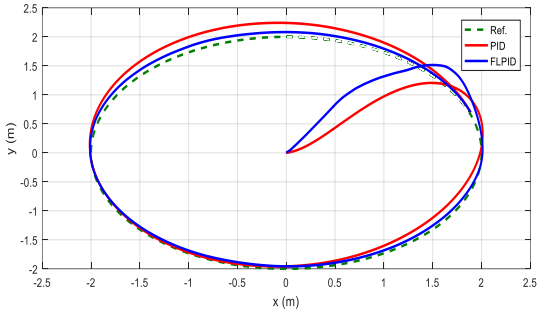

Figure 10. An x-y plan circle path scenario. PID controller output is displayed as red, FLPID controller output as blue, and the desired path is displayed as a green dashed line

Table 9. Controller gain parameters

position	Tuned		Untuned		velocity	Tuned	Untuned
	Kp	Ki	Kp	Ki		Kd	Kd
x	10.27	0	10	0	u	17.32	17.8
y	0.76	0.088	0.71	0.1	v	1.68	1.7
z	13.27	0	15	0	w	26.44	30.5
Ψ	198.74	0	200	0	r	90	90

Figure 11. 3D space path scenario. PID controller output is displayed as red, FLPID controller output as blue, and the desired path is displayed as a green dashed line.

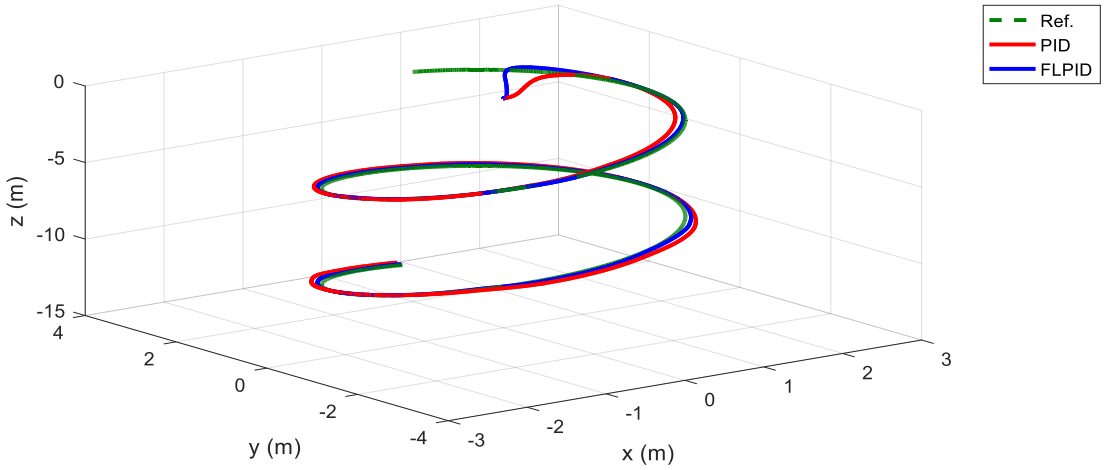

The time-dependent changes of position in the x and y directions as the vehicle follows the trajectories and the angular displacement of the vehicle around the z-axis are shown in figures 12, 13 and 14.

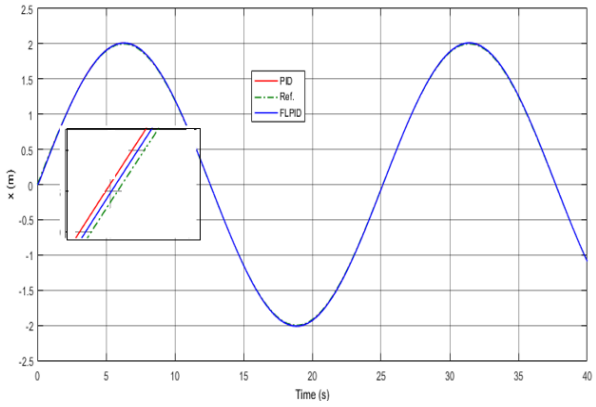

Figure 12. Change in x location over time for following a circular journey. The intended trajectory is shown by the green dashed line, the blue line represents the output of the FLPID controller, and the red line represents the PID controller's output.

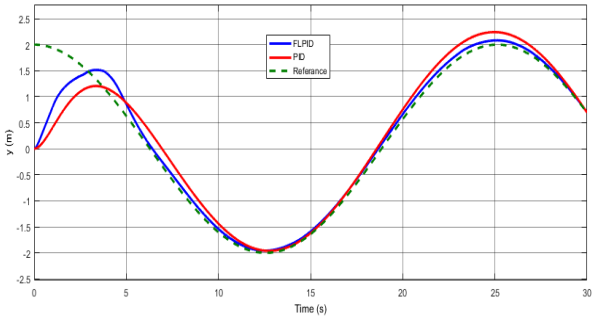

Figure 13. Y position variation over time for following a circular path. The intended trajectory is shown by the green dashed line, the blue line represents the output of the FLPID controller, and the red line represents the PID controller's output.

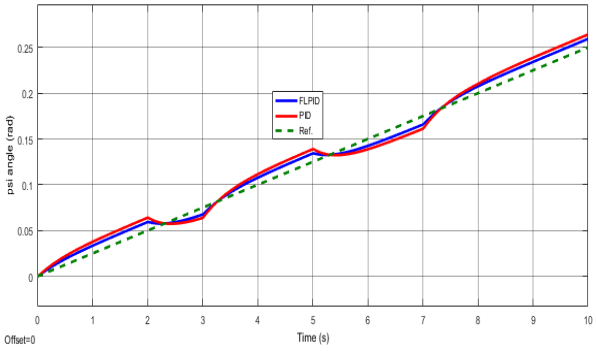

Figure 14. yaw angle variation over time for monitoring circular paths in the x-y plane.

The average values of the position errors (in the x, y, and z axes) over time, occurring while the underwater vehicle follows a 3D spiral trajectory, are shown in Table 10.

The time-dependent variations of the position errors in the y and z axes for both controllers are depicted in Figure 15. As the difference in position errors for surge freedom is not significantly pronounced (see Figure 12), the position error along the x-axis is not shown.

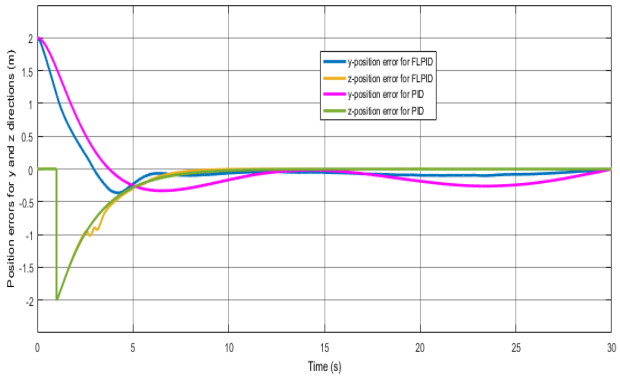

Figure 15. The position errors in the y and z components for PID and FLPID

Table 10. The mean values of position errors

	Mean position errors		
Controller	x-direction	y-rection	z-irection
PID	0.000156m	0.157 m	0.043 m
FLPID	0.000106 m	0.152 m	0.022 m

In all simulations, a band-limited white noise signal of 0.05W with a sampling frequency of 0.1s was used as environmental disturbance.

VI. CONCLUSIONS

In this article, after modeling a UUV based on dynamic principles and verifying the model, trajectory tracking control is presented using a self-tuning fuzzy PID controller. In the proposed approach, the FLPID controller has two inputs. One input signal is the system error function, which is proportional to the traditional PID parameters K_p, K_i, K_d, and the other is the time derivative of this error. During the operation of the PID controller based on initial optimization, the parameters K_p^0, K_i^0, and K_d^0 are kept constant. The performance of the proposed controller is examined through simulations conducted using SimulinkTM. This study considers practical requirements for real-world implementation. Simulation results demonstrate that the adaptability and robustness of the FLPID controller are superior to the equivalent PID controller. Furthermore, the suggested FLPID controller's ability to enhance robustness can be observed in terms of the average values of time-varying position errors. Today, fuzzy logic and PID controllers are easily applied in various industries through microcontrollers or mini-PLCs, making the implementation of this controller straightforward.

In future research, the aim is to investigate the controllability and accessibility of the entire control system by integrating advanced metaheuristic-based approaches to optimize control gains and validate the proposed algorithms for a UUV prototype through further testing in open water.

ACKNOWLEDGEMENT

This study was supported by Kocaeli University Scientific Research Projects Coordination Unit. Project Number: FDK-2022-3008. We thank the unit for their support.

REFERENCES

[1] Sahoo, A. Dwivedy, S. K. and Robi, P. S. (2020). Adaptive Fuzzy PID Controller for A Compact Autonomous Underwater Vehicle. in *Global Oceans Singapore – U.S. Gulf Coast*, Biloxi, MS, USA: IEEE

[2] Chin, C. and Lau, M. (2012). Modeling and testing of hydrodynamic damping model for a complex shaped remotely-operated vehicle for control. *J. Marine. Sci. Appl.*, vol. 11, no. 2, pp. 150–163

[3] Fossen, T. I. (1994), Guidance and control of ocean vehicles. Wiley, New York

[4] Fossen,T.I.(2011). Handbook of Marine Craft Hydrodynamic and Motion Control, Wiley, New York

[5] Hammad, M. M. Elshenawy, A. K. and El Singaby, M. I. (2017). Trajectory following and stabilization control of fully actuated AUV using inverse kinematics and self-tuning fuzzy PID. *PLoS ONE*, vol. 12, no. 7

[6] Stipanov, M., Miskovic, N., Vukic, Z., and Barisic, M. (2007). Rov Autonomızatıon Yaw Identıfıcatıon And Automarıne Module Archıtecture. *IFAC Proceedings Volumes*, vol. 40, no. 17, pp. 175–180

[7] Cely, J., S., Salteren, R., Portilla, G., Yakrangi, O., and Barroso, A. R. (2019). Experimental and Computational Methodology for the Determination of Hydrodynamic Coefficients Based on Free Decay Test: Application to Conception and Control of Underwater Robots. *Sensors*, vol. 19, no. 17, p. 3631

[8] Carrasco, G. R., Viedma, A. and Toledo, A. C. (2015). Coefficient estimation in the dynamic

equations of motion of an AUV. *Sıxth Internatıonal Workshop On Marıne Technology, Martech*

[9] Amini, F. J., Sabzpooshani, M.(2021), An Approach for the Estimation of Hydrodynamic Coefficients of an Underwater Vehicle in Off-Design Velocities.
J. Mar. Sci. Technol. 2021, 26, 368–381

[10] Phillips, A., Furlong, M., Turnock, S.R. (2022), The Use of Computational Fluid Dynamics to Determine the Dynamic Stability of an Autonomous Underwater Vehicle, https://eprints.soton.ac.uk/48786/1/ABP_NUTTS.

[11] Ataei, M. and Yousefi-Koma, A. (2014), Development of a Three-Dimensional Guidance System for Long-Range Maneuvering of a Miniature Autonomous Underwater Vehicle, *China Ocean Eng*, vol. 28, no. 6, pp. 843–856

[12] Xin, Z. (2013). Parameter Optimization of PID Controller Based on PSO for Multi-leaf Collimator. *Telkomnika*, vol. 11, no. 10, pp. 6127–6134

[13] Yu, C., Xiang, X. and Dai, J. (2016). 3D path following for under-actuated AUV via nonlinear fuzzy controller. in *OCEANS 2016 - Shanghai*, Shanghai, China: IEEE, Apr. 2016, pp. 1–7

[14] Sarhadi, P. Noei, A.R, Khosravi, A. (2016) Model reference adaptive PID control with anti-windup compensator for an autonomous underwater vehicle. Robotic and Auton., vol. 83. P. 87–93

[15] Nguyen, D. A., Thanh, D. D., Tien, N. T. and Anh, P. V., Fuzzy Controller Design for Autonomous Underwater Vehicles Path Tracking, *International Conference on System Science and Engineering (ICSSE)*, Dong Hoi, Vietnam: IEEE, Jul. 2019, pp.–598

[16] Fangui, M., Liu, A., Jing, S. and Zu, Y., FSM trajectory tracking controllers of OB-AUV in the horizontal plane, in *2021 IEEE International Conference on Intelligence and Safety for Robotics (ISR)*, Tokoname, Japan: IEEE, Mar. 2021, pp. 204–208

[17] Xie, J., Chen, M. and Zhu, D., A cascaded model predictive control based trajectory tracking controller for an autonomous and remotely operated vehicle with LOS guidance, *Ships and Offshore Structures*, pp. 1–15, Sep. 2023

[18] Gonzalez, J., Gomariz, S., Batlle, C. and Galarza, C., Fuzzy Controller for the yaw and velocity control of the Guanay II AUV., IFAC-Papers OnLine, 2015 Sep;48(6):2682

[19] Wang, Y., Shen, Y., Wang, K. And Sha, Q., Fuzzy Controller Used Smoothing Function for Depth Control of Autonomous Underwater Vehicle, OCEANS, 2016 April;(5)

[20] Sahoo, A., Dwivedy, S. K., Robi, P. S. (2020), Dynamic Modelling and Control of a Compact Autonomous Underwater Vehicle. in Lecture Notes in Mechanical Engineering. Singapore: Springer Singapore, pp. 303–321. doi: 10.1007/978-981-13-8323-6_25

[21] Boiocchi R,, Gernaey K.V. and Sin G., Systematic design of membership functions for fuzzy-logic control: A case study on one-stage partial nitritation/anammox treatment systems. Water Research. 2016 Oct; 102(10):346. https://doi.org/10.1016/j.watres.2016.06.047 PMID: 27390035

[22] Fossen, T.I. and Fjellstad, O.E., Nonlinear Modelling of Marine Vehicles in 6 degrees of Freedom, International Journal of Mathematical Modelling of Systems. 1995; 1(6)17. https://doi.org/10.1080/ 13873959508837004

[23] MitrasThruster, Degz Robotics, Last Accessed, 11 April 2022, https://degzrobotics.com/mitras-itki-testleri/